PATTERNS FORMATION IN A PMZC PLANKTON MODEL

Tahani Al-Karkhi

Department of Mathematical Sciences, University of Essex, UK

Wivenhoe Park, Colchester, CO4 3SQ, United Kingdom

Abstract

In this paper, we focus on the phenomenon of pattern formation in a reaction diffusion model of plankton dynamics, which includes support for infochemically mediated trophic interactions. We consider a four species model created on the basis of the two species models which have been studied previously. In our model, which is an extended version of these previous models, the grazing pressure of microzooplankton (M) on phytoplankton (P) is controlled through external infochemically (C) mediated predation by copepods (Z). We undertake a stability analysis of both the two species and the four species models and compare their system dynamics. We compared the mathematical roots related to these models using both numerical and analytical methods, and we found consistency between the two approaches using asymptotic expansion. We also explored spatial pattern formation in relation to both forms of model and considered under what conditions Turing patterns are exhibited and when spatiotemporal chaos can be observed. An attempt was made to study the non-Turing patterns, which were discovered with a special emphasis on spatiotemporal chaos.

***Keywords**:*

Plankton model, Plankton dynamics, Infochemicals, PMZC-model, Asymptotic Expansion Analysis, Limit cycle, Dynamical system, Chaos, Systematic analysis, Food-webs, Multitrophic interactions.

1. Introduction

As highlighted by (Banerjee, 2015), Turing and non-Turing Patterns have been used by many researchers to try to understand the mechanisms of pattern formation in various physical processes. Turing and non-Turing Patterns arise, in the biological context, as a result of interactions between different species, leading to the modification of the temporal dynamics of population distributions (Bandyopadhyay and Chattopadhyay, 2005). Among the processes which instigate such pattern formation are, for instance, the meanderings of rivers; the mixing of chemical reagents and chemical processes; and ripple like structures in the sand (Banerjee, 2010). In this work, we introduce the trophic web illustrated in Fig.(1), where the arrows

indicate the interaction directions. There are four interacting components, namely the phytoplankton (P), the microzooplankton (M), the zooplankton (Z), and the infochemical release, (C) as shown in Fig.(1). The interactions shown in the diagram are described by a system of four differential equations, below is a full description of the PMZC-model.

$$\frac{\partial \overline{U}}{\partial t} = D_i \nabla^2 \overline{U} + F_i(\overline{U})$$

Where U represents a vector of four components: P denotes the population density of the prey phytoplankton, M denotes the population density of the predator microzooplankton, and Z denotes the population density of the top predator (copepods), all at time T; i = 1,2,3,4 indicates the num-

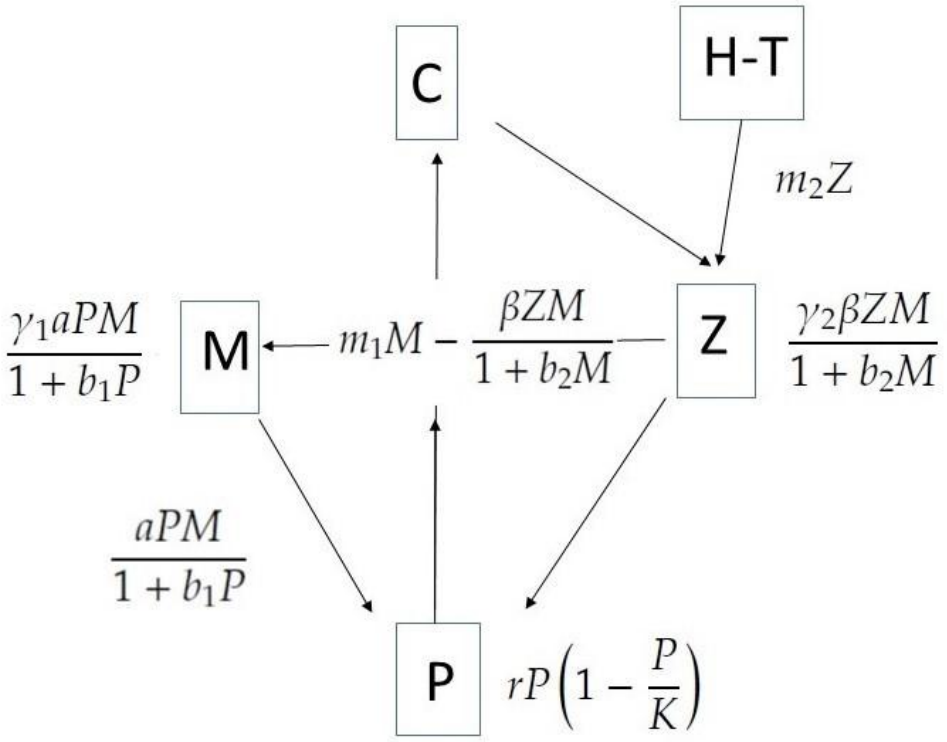

Figure 1: Schematic diagram of proposed model

ber of species in the community, C denotes the effect of prey (copepods) on trophic interactions, and functions F_i take into account the effects of birth and mortality. In most biologically meaningful situations, the functions F_i are nonlinear with respect to at least some of their arguments. In the second part of the above equation, $D\nabla^2 U$ indicates that the simplest (biologically meaningful) case is yielded by random isotropic motion, i.e., diffusion, where D_i is the diffusion coefficient of the ith species, and ∇^2 is the Laplace operator:

$$\nabla^2 = \frac{\partial^2}{\partial x^2} + \frac{\partial^2}{\partial y^2} \quad (2)$$

Keeping in view the above discussion, we study a plankton model supporting a one prey and two-predator system with Holling type *II* functional responses Fig.1. The main contribution of this paper is to expand the two trophic model studied by (Lewis et al., 2012) to a four trophic model and then study the effect of diffusion on the resultant four species food web model (which retains the Holling type *II* functional responses).

We focus mainly on a spatiotemporal system and provide an analytical and numerical explanation of diusion driven instability conditions. The Non-Turing patterns encountered are studied with particular emphasis on spatiotemporal chaos, which can explain the irregular distribution of populations so frequently observed in nature. Phytoplankton, which plays a crucial role in ocean dynamics, forms the basis of all food sources in aquatic environments (K et al., 1992). Zooplankton consumes phytoplankton, and this interaction forms the basis of the prey predator associations in marine environments. Phytoplankton supplies oxygen and absorbs carbon dioxide, thus combating global warming effects (Edwards and Brindley, 1999). Infochemicals play a vital role in food web interactions; they can help prey to avoid predators, and conversely they can assist predators to locate prey. Infochemicals can also assist in the location of mates (Banerjee, 2010). Phytoplankton have trophic interactions, which help them defend themselves against grazers. These involve the use of deterrents and toxins, as well as multi-trophic interactions that indirectly influence the foraging behaviours of prominent predators (predators of those species which prey on phytoplankton) (Banerjee and Venturino, 2011). It is crucial to study marine ecosystems because they are central to the mechanisms by which life on earth maintains itself. Studies of predator-prey models have developed from looking at one, two and three species models to looking at four and n species models, although there is little research on the latter. The methodology has been developed using mathematical equations originated by the pioneers (Rosenzweig and MacArthur, 1963) and (Edwards and Brindley, 1999). The simple population model as developed by (Maini et al., 2012) illustrates phytoplankton that produce DMS in small quantities a one species model. When grazing by microzooplankton is added, this becomes a two species model and when microzooplankton predations by mesozooplankton is added, a three species model. The above study was based on an initial assumption that microzooplankton act as a trophic link between plankton and copepods. DMS (Dimethylsulde) is well studied due to its potential impact on climate regulation (E et al., 1987), but it is also increasingly being recognized as an important marine infochemical, with a number of studies reporting that it results in attraction by a wide range of taxa (Baurmann et al., 2004). The release of DMS (Dimethylsulde) is promptly accelerated following microzooplankton grazing on phytoplankton (S et al., 2016), and this release is shown to elicit a behavioural foraging response in the copepod Temora longicornis (Wolfe and Steinke, 1996), making this copepod a relevant example for this study. The four species prey-predator model developed in this study is based on the multi-trophic interactions that are exhibited once infochemicals are released after microzooplankton start grazing on phytoplankton; the released chemical cues attract copepods that prey on microzooplankton, thus inducing significant grazing pressure (on the latter). These interactions form the basis of the four species model. Here we construct a PZC-style model which supports two species of zooplankton, microzooplankton and copepods; this yields a PMZC model. First, we study the dynamic behaviour of the system under varying levels of infochemically mediated predation and then we examine how the system changes as the levels of a number of different resources are varied simultaneously. Also, we study the behaviour of the system once spatial considerations have been added, and we carry out a Turing instability analysis in order to determine the robustness of the resultant model, as recent

studies in the ecological field pay particular attention to the practical contexts of spatial processes (Baurmann et al., 2004). The remainder of this paper is organized as follows: in Section 2, we propose the spatiotemporal PMZC model; Section 3 presents an asymptotic expansion analysis; this is followed by Section 4 which presents a local stability analysis and indicates the limit cycle condition for the temporal system; In Section 5, we derive the analytical conditions for diffusion driven instability using the Ruth Hurwitz criteria. Also in that section we provide the results of the numerical simulation, which was performed; in Section 6, the systematic analysis is discussed; and finally, conclusions are given in the last section, Section 7.

2. The temporal PMZC-Model

A mathematical model was developed of the situation whereby one prey species is utilized by two predator species and this model included the chemical releases involved; this was studied within a temporal domain and with Holling type *II* functional responses (Holling, 1965). Motivated by the work (Lewis et al., 2012), we derived F_i, i = 1..4, which is the interaction function for the model which we have developed. The interaction function has the following format:

,

$$\frac{dP}{dt} = F_1(P, M, Z, C) \quad (3)$$

$$\frac{dM}{dt} = F_2(P, M, Z, C), \quad (4)$$

$$\frac{dZ}{dt} = F_3(P, M, Z, C), \quad (5)$$

$$\frac{dC}{dt} = F_4(P, M, Z, C). \quad (6)$$

$$F_1(P, M, Z, C) = rP\left(1 - \frac{P}{K}\right) - \frac{aPM}{1 + b_1 P}, \quad (7)$$

$$F_2(P, M, Z, C) = \frac{\gamma_1 aPM}{1 + b_1 P} - m_1 M - \frac{\beta\ ZM}{1 + b_2 M}(1 + \frac{\zeta C}{1 + \epsilon C}) \quad ,(8)$$

$$F_3(P, M, Z, C) = \frac{\gamma_2 \beta\ ZM}{1 + b_2 M}(1 + \frac{\zeta C}{1 + \epsilon C}) - m_2 Z, \quad (9)$$

$$F_4(P, M, Z, C) = \frac{\eta aPM}{1 + b_1 P} - m_3 C + \omega P. \quad (10)$$

The above model describes the interactions between the small infochemical producing phytoplankton, the microzooplankton and the copepods in a system that is depleted of nutrients. The parameter, *r*, represents the phytoplankton intrinsic growth rate, *a* is the clearance rate of microzooplankton at low food densities, b_i i = 1,2 represents the half saturation constants, β is the copepod linear predation rate, m_i (i = 1,2) are the predators death rates, m_3 is the chemical evaporation rate, γ_i i = 1,2, are the parameters representing the biomass conversion rates, from prey to predator. ζ is the rate of chemical change

and is a key parameter that we use to reduce the general four species model to a special case model, i.e., that of (Lewis et al., 2012). η is the productivity rate of the DMS-infochemicals, and ω is the amount of chemical given off by each phytoplankton. In Eq. (7), we employ a logistic map to describe the growth rate of prey and a Holling II functional response to describe the effects predators have on (the microzooplankton) prey. In Eq. (8), we define the microzooplankton population growth using a Holling II functional response with γ_1 as a conversion parameter — this latter regulates the conversion of prey biomass into predator biomass. The second term in Eq.(8) represents the normal (non-predator-induced) mortality of microzooplankton, while the third term represents the effects of zooplankton on microzooplankton— of course, zooplankton provides another source of microzooplankton mortality. The third term represents the increase in predation with β as a linear predation rate [1]. Copepods saturate w.r.t. their predation activities according to their behaviour when handling their prey (microzooplankton), with b_2 being the half saturation parameter. The chemicals released could also be saturated via the (1 + C) factor, and the ζ parameter is used to measure the rate of chemical increase (that effects increases in predation [2]. In Eq. (9) the first term we introduce is the copepod population growth which connects both predator populations, M and Z. This term also describes how copepods consume microzooplankton following *DMS* release and how copepods saturate because of the time it takes to handle prey. The next term represents copepod mortality due to their consumption by higher trophic predation. The final equation (10) has three terms. The first term is used to describe the infochemical release following the start of microzooplankton grazing on phytoplankton; η is the productivity rate of *DMS*. The second term in F_4 stands for chemical evaporation. The third term represents the level of chemical (exudation) release by each cell. We can reduce the model in Eqs. (7)- (10) into a special case model by setting $\epsilon = 0, b_2 = 0, \omega = 0$, i.e:

$$F_1(P, M, Z, C) = rP\left(1 - \frac{P}{K}\right) - \frac{aPM}{1 + b_1 P} \tag{11}$$

$$F_2(P, M, Z, C) = \frac{\gamma_1 aPM}{1 + b_1 P} - m_1 M - \beta ZM(1 + \zeta C) \tag{12}$$

$$F_3(P, M, Z, C) = \gamma_2 \beta ZM(1 + \zeta C) - m_2 Z \tag{13}$$

$$F_4(P, M, Z, C) = \frac{\eta aPM}{1 + b_1 P} - m_3 C \tag{14}$$

The main difference between the two set of nonlinearities and the model represented by Eq. (14) is the linear predation function, which describes the linear effects of the predation by copepods of microzooplankton. It can be assumed that the

[1] -β MZ represents the effects of the copepods on the microzooplankton; any species should saturate at some level. Therefore we changed the layout of this term to that of a
Holling II functional response.

[2] $\left(\frac{\zeta C_{max}}{1+C}\right)$ also can be defined as the maximum level of chemical, which can be released, especially if we model this term by 1 + ζ.

model is valid over significant periods of time–scales because we have included resources which are in addition to the basic food chain of the two species model: i.e., the infochemical releases (by the phytoprotozoa) and the population density of the copepods. Thus, we must consider the time that both predators *M* and *Z* take to handle their prey. The model represented by Eq. (14) is considered as a special case of the models represent by Eqs. (7) - (10). This is because, when $\epsilon = b_2 = \omega = 0$ the model is reduced to the two species model as in (Lewis et al., 2012). One goal of the model construction undertaken here is to predict the predator–prey kinetic and dynamic properties. Since our model is constructed from the two species predator–prey model *P* and *M*, a basic question to raise here is how can the four species model provide for more descriptive power than the two species model?

3. Qualitative analysis of the location of the equilibria

Here we look for the steady-state solutions (*P*,*M*,*Z*,*C*) which satisfy $(\frac{dp}{dt}, \frac{dM}{dt}, \frac{dZ}{dt}, \frac{dC}{dt}) = 0$. The system shown in Eqs. (7)-(10) possesses five possible nonnegative equilibria: namely, the extinction equilibrium E_0; the microzooplankton and copepod-eradication equilibrium E_1; the phytoplankton and infochemical eradication equilibrium E_2; the copepod (free) eradication equilibrium E_3; and finally the coexistence equilibrium E_4. Table 3 shows the number of equilibria and their types and definitions.

Table 1: All possible equilibria of the system given by Eqs. (7)-(10) both biologically relevant and irrelevant.

Equilibrium	Definition	Value in Parametrized System	Description	Hyperbolic Eigenvalues
E_0	(P_e,M_e,Z_e,C_e)	(0,0,0,0)	Trivial (extinct)	Eq. (20)
E_1	(P_e,0,0,C_e)	$(K, 0, 0, \frac{K\omega}{m_3})$	phytoplankton and infochemical equilibrium	Eq. (21)
E_2	(0,M_e,Z_e,0)	(0,M_e,Z_e,0)	Biologically irrelevant equilibrium yielded by Eq (15)	Eq.(22)
E_3	(P_e,M_e,0,C_e)	(*P*,*M*,0,*C*)	Copepod free equilibrium yielded by Eq (16)	Eqs. (23).
E_4	(P_e,M_e,Z_e,C_e)	as in Eq (17)	Full Coexistence equilibrium yielded by Eq. (17)	Eqs.(17)

The biologically irrelevant equilibrium is yielded by:

$$E_2 = (0, \frac{m_2}{\beta(\gamma_2)}, \frac{-\gamma_2 m_1}{\beta(\gamma_2)}, 0). \quad (15)$$

The fourth equilibrium is yielded by:

$$E_3 = \left(\frac{m_1}{(a\gamma_1 - b_1 m_1)}, \frac{r\gamma_1(aK\gamma_1 - Kb_1m_1 - m_1)}{K(a\gamma_1 - b_1 m_1^2)}, 0, \frac{(a\eta Kr\gamma_1 - \eta Krb_1m_1 + aK\omega\gamma_1 - K\omega b_1 m_1 - \eta r m_1)}{(K(a\gamma_1 - b_1 m_1)^2)}\right). \quad (16)$$

The full co-existence state satisfies the quartic polynomial

$$\sum_{i=0}^{4} A_i P_e^{4-i} = 0, \quad (17)$$

Where A_i, i = 0,..,4 are cascading parameters as given in Appendix A. While M, Z and C are given by

$$M(P_e) = \frac{-r}{aK}\left(b_1 P_e^2 - (Kb_1 - 1)P_e - K\right),$$

$$Z(P_e) = A_5(P_e)^2 + B(P_e) + G, \quad (18)$$

$$C(P_e) = \frac{(P^2\eta r - P\eta Kr - K\omega)}{(Km_3)}.$$

The persistent full co-existence is state yielded by a quartic polynomial as follows;

$$\sum_{i=0}^{4} A_i P_e^{4-i} \quad (19)$$

Where A_i, i = 0,..,4 are all cascading parameters (provided in Appendix C).

3.1. System behaviour near the origin E_0

A straightforward calculation shows that the hyperbolic equilibrium, which is the first trivial (extinction) equilibrium, is an unstable saddle point, with the unstable manifold in the direction orthogonal to the $M-Z-C$ coordinate plane.

$$\lambda_{E0} = (r, -m_1, -m_2, -m_3) \quad (20)$$

3.2. System behaviour near the microzooplankton and copepod eradication equilibrium E_1

The E_1 equilibrium point of the system, which entails microzooplankton and copepod eradication, is locally asymptotically stable if $\gamma_1 ak - b_1 km_1 - m_1 \leq 0$. Further, if $\gamma_1 ak < b_1 km_1 - m_1$, $1 + b_1 k > 0$ then E_1 is globally

stable. The eigenvalues of the second microzooplankton and copepod eradication equilibrium are:

$$\lambda_{E_1} = (-r, \frac{\gamma_1 ak - b_1 km_1 - m_1}{1 + b_1 k}, -m_2, -m_3) \qquad (21)$$

3.3. System behaviour near the phytoplankton and infochemical eradication equilibrium E_2

The Jacobian matrix of the system 10 around the, non-feasible, phytoplankton and infochemical eradication equilibrium point, E_2, yields the following eigenvalues.

$$\lambda_{E_2} = (\frac{\gamma_2 \beta r - b_2 m_2 r - am_2}{\gamma_2 \beta - b_2 m_2}, \frac{1}{2A_0}(\alpha \mp \sqrt{\beta}), -m_3), \qquad (22)$$

Where all its coefficients are given in Appendix **3** Now, this hyperbolic point is an unstable saddle, since all the parameters are positive: λ_1 is unstable; also, because $\lambda_{2,3}$ have negative real parts, these are stable foci. Further, since $\lambda_4 < 0$ we have a saddle-focus point, as when we have one real eigenvalue with the opposite sign to that of the real part of a pair of complex-conjugate eigenvalues and a negative real fourth eigenvalue; This type of equilibrium is always unstable.

3.4. System behaviour near the copepod eradication equilibrium E_3

The Jacobian matrix of the system 10 for the fourth equilibrium (with copepod eradication) has the following four eigenvalues:

$$\lambda_1 = \frac{A}{B} \qquad (23)$$

Where A and B are as in Appendix **2.** This hyperbolic point is unstable since all the parameters are positive. And λ_1 is unstable if $A > B > 0$, and because $\lambda_{2,3}$ have negative real parts, these are stable foci, and since $\lambda_4 < 0$, we have a saddle-focus point — as when we have one real eigenvalue with the opposite sign to that of the real part of a pair of complex-conjugate eigenvalues and a negative real fourth eigenvalue; This type of equilibrium is always unstable.

3.5. System behaviour around the coexistence equilibrium point E_4

The relevant Jacobian matrix is $J_4 = (a_{ij})_{4\times4}$. Let λ_i, i = 1,2,3,4 be the roots of the characteristic polynomial of J_4 which is given by:

$$\sum_{i=0}^{4} A_i \lambda^{4-i} = 0 \qquad (24)$$

,

Where A_i are cascading parameters given in Appendix D and $A_0 = 1$. From the Routh-Hurwitz criterion, all the roots of a Jacobian matrix have negative real part if and only if the determinants of all the Harwitz matrices are positive (Porter, 1968), and then any E is locally asymptotically stable if and only if $A_1 > 0$, $A_3 > 0$ and $A_1A_2 > A_3$ and $A_3 > {}^{p}A_1(A_1A_4 - A_2A_3)$ or $A_1A_2A_3 > A_3^2 + A_1^2A_4$.

Obviously, we have $A_1 < 0$ and $A_3 < 0$ and by depending on the Jacobian element matrix, when $a_{12} < 0$, $a_{21} > 0$, $a_{23} < 0$, $a_{32} > 0$, $a_{33} < 0$ and $a_{44} < 0$. It is readily seen that $A_1A_2A_3 > A_3^2 + A_1^2A_4$. Therefore, we formulate the necessary and sufficient conditions for the positive equilibrium to be locally asymptotically stable; these follows from the Routh Hurwitz criterion. For this purpose, we use the notation given in appendix.

4. Asymptotic Expansion Analysis

Using an asymptotic approach it is possible to make some limited analytical progress with the general system given in Eqs.(10). In this analysis, we study how to scale our parameters in order to determine the general stability for PMZC-models' roots. We can start performing the method by setting the following assumption: $k = \frac{\widehat{k}}{\epsilon^2}$, $\widehat{a} = \frac{a}{\epsilon}$, $\widehat{b_1} = \frac{b_1}{\epsilon^2}$, $\widehat{b_2} = \frac{b_2}{\epsilon^2}$, $\widehat{m_1} = \frac{m_1}{\epsilon}$, $\widehat{m_2} = \frac{m_2}{\epsilon}$, $\widehat{m_3} = \frac{m_3}{\epsilon}$, $\eta = \frac{eta}{\epsilon}$, $\gamma_1 = \frac{\gamma_1}{\epsilon}$, $\gamma_2 = \frac{\gamma_2}{\epsilon}$. and by substitute our scaled parameters and the following expansion into the full co-existence persistence state, which is given by 17:

$$P = \frac{P_0}{\epsilon^2} + \frac{P_1}{\epsilon} + P_2 + \ldots \tag{25}$$

we will obtain an expanded polynomial, by collecting the coefficient of its leading order we could obtain the appropriate value of prey density P_e. Which is:

$$P_{E_4} = \frac{\widehat{k}}{\epsilon^2} \tag{26}$$

and by substituting the expanded (scaled) value of P into the quadratic polynomial of *MZC*, we could have the following values for the predators *MZ* and chemical release *C*.

$$M_{E_4} = \frac{1}{\widehat{a}\epsilon}$$

$$Z_{E_4} = \frac{-\zeta\eta^2 r\widehat{k}\widehat{\gamma_2}b_1m_3(\widehat{k}\gamma_2b_1 + \widehat{k}b_1 + \gamma_2 + 1)}{\epsilon}$$

$$C_{E_4} = \frac{\widehat{\eta}\widehat{k}r}{m_3}.$$

Now, after determine the values of scaled root E_4, we could study the general stability analysis by following the same procedures method we presented on this section i.e

$$\lambda_{E_4} = \frac{\lambda_0}{\epsilon} + \frac{\lambda_1}{+}... \tag{27}$$

An expanded characteristic polynomial could be obtained following the same procedures and by substituting 27 and collecting the coefficient of the leading order and then solve for λ, we could obtain the following eigenvalues:

$$\lambda_{E_4} = (0, 0, \frac{\widehat{\gamma_1}\widehat{a}}{\widehat{b_1}}, \frac{\widehat{\zeta} + \widehat{\gamma_2}}{\widehat{b_2}}). \tag{28}$$

and by substituting the analytically derived value of P into the quadratic polynomials of M and C and the fractional polynomial of Z we obtain:

$$M_{E_4} = \left(\frac{\widehat{k}\widehat{b_1}\widehat{a}}{\widehat{a}\widehat{\zeta}(\widehat{b_1}\widehat{k}+1)} + \frac{\widehat{m_2}\widehat{a}}{\widehat{a}\widehat{\zeta}(\widehat{b_1}\widehat{k}+1)} \right) \epsilon$$

$$Z_{E_4} = \frac{\widehat{a}\widehat{k}\widehat{m_3}\widehat{\gamma_1}}{(\widehat{b_1}\widehat{k}\widehat{m_3} + \widehat{k}\widehat{m_3}\beta)}$$

$$C_{E_4} = \frac{\widehat{\eta}\widehat{k}r}{\widehat{m_3}}.$$

After determining the values of the scaled root, E_4, we can undertake a general stability analysis by following the same procedures. After determining the characteristic polynomial of the model in Eq. 6 from the Jacobian matrix, we expand λ as in Eq. 29and substitute it back into the characteristic polynomial.

$$\lambda = \frac{\lambda_0}{\epsilon^2} + \frac{\lambda_1}{\epsilon} + \lambda_2 + ... \tag{29}$$

and by collecting the coefficient of the leading order, we will determine four eigenvalues as follows:

$$\lambda_{1,2} = \frac{A}{B},$$

$$\lambda_{3,4} = \frac{1}{2A_0}(\alpha \mp \sqrt{\beta})$$

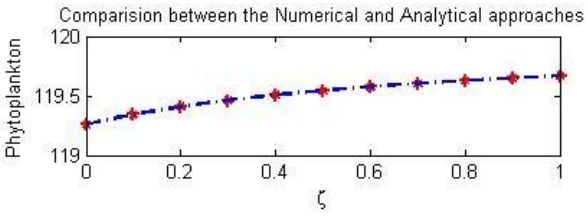

Figure 2: A comparison between the numerical and the analytical approaches used to solve the quantic polynomial of the four species model in Eq.6.

Where A, B, α and β are all cascading parameters: the formula is quite prolix, so it has been moved to the appendix. Comparing the analytical roots and eigenvalues of the system, 6, with the numerical results shows that all the results are consistent. Fig. 2 illustrates the consistency of the two approaches.

5. Parameter Values Investigation

A major reason for modelling the dynamics of a population is to understand its principle controlling features and so be able to predict the likely pattern of development consequent upon a change of environmental parameters (Murray, 2002). In the PMZC model of 10 we assumed that the parameters within the elementary analysis are similar to their values as given previously (Lewis et al., 2012).We denote these values as default values. It was apparent that oscillatory solutions were present in the two models, when $\kappa = b2 = \omega = 0$ and when $\kappa = 1$, $b_2 = 0.05$, $\omega = 0.1$; this makes the two sys-
tems presented here consistent with the results which were found previously:

i.e. the model relaxes to a stable steady state. However, in this paper we are concerned with a 4 species system. Therefore, we need to consider carefully the effects of each parameter on the PMZC food chain; this might help us to obtain a valid solution (model) especially with respect to the fact that we are introducing the effects of zooplankton into this system. Following (Edwards and Brindley, 1999), the parameter values used to model the zooplankton mortality can have a major influence on the dynamics of simple models (Edwards and Yool, 2000), (Edwards and Brindley, 1999). They found that, for their particular parameter values, the limit cycle behaviours (unforced oscillations) which occurred when they used a linear zooplankton mortality term did not occur when they used a quadratic term. With respect to (Lewis et al., 2012) and (Morozov et al., 2010), we keep the maximum growth rate parameter of these logistic growth models in the range $0.1 < r < 2d^{-1}$. In (Franks, 2001), the phytoplankton carrying capacity was set to $K = 50\mu gCI^{-1}$, but (Morozov et al., 2010) considered a much wider range $K = \infty$. Therefore, we use $50 < K < \infty$ (Edwards and Brindley, 1999).

(Edwards and Brindley, 1999), (Saiz and Calbet, 2007) estimated the half saturation constant of phytoplankton to be in the range $20 < b_1 <$
$150\mu gCI^{-1}$, and the zooplankton (copepod) half saturation constant to be $20 < b_2 < 100\mu gCI^{-1}$ — to reflect the fact that copepod dynamics develop on a slower time scale than microzooplankton dynamics. However, because we are introducing zooplankton (copepods) and we are going to study their effects on the food chain, the more accurate values for b_1 and b_2 which will be used in this model is much smaller than the literature suggests. We will set a very small value for the zooplankton (copepod) population density, in contrast to that set for microzooplankton. This is because we are not introducing any higher trophic, and because the model is non-nutrient limited in particular circumstances. We have chosen the b_1P and b_2M terms in the way that we have because these terms may be regarded as reflecting the amount of time it takes for the predators to handle their prey (Cantrell and Cosner, 2004), and if we choose $\frac{\gamma_1 a}{b_1} - m_1 > 0$, then the predator density will tend to zero over time. Therefore, we postulate that $\frac{\gamma_1 a}{b_1} > m_1$ similarly for

$\frac{\gamma_2 \beta}{b_2} > m_2$. In this model, we cannot choose $b_2 > b_1$ for the same reasons.

In (Strom and Morello, 1998), the microzooplankton conversion efficiency is estimated to be $0.15 < \gamma_1 < 0.64$, but (Kiørboe, 2008) states that the conversion efficiency may be higher when considering zooplankton feeding on microplankton; hence, here, a higher value of $\gamma_2 = 0.7$ is chosen for the copepod assimilation efficiency. Also, the maximum copepod predation rate was chosen to be $\beta = 1d^{-1}$. In our model, copepods are specified as having a default mortality value; we didn't take into account any predation from higher predators which would increase this above the rate of mortality due to old age, etc. We can determine the effects of choosing these specific values numerically by substituting the default values from table 2 into the functional responses to check the corresponding population density. Here we present the parameter values that have been used in the current study:

Table 2: Outline descriptions, default values and the ranges of the parameters: the ranges presented cover values used by a variety of authors for different models.(Edwards and Brindley, 1999), (Edwards and Yool, 2000) and (Saiz and Calbet, 2007).

20

Parameters	Definition	Value	Unit	Range
R	Phytoplankton Intrinsic Growth rate	1.5	$days^{-1}$	
K	Phytoplankton Carrying Capacity	120	$\mu g\ C\ I^{-1}$	
A	Clearance Rate of Microzooplankton at Low Food Densities	0.3	$\mu g\ CI^{-1}\ days^{-1}$	
b_1	Half Saturation Density	0.05	$\mu g\ C\ I^{-1}$	0.01 − 0.05
b_2	Half Saturation Density	0.02	$\mu g\ C\ I^{-1}$	0.01 − 0.05
γ_1	Microzooplankton Grazing Efficiency	0.3	$days^{-1}$	0.3 − 0.64
γ_2	Mesozooplankton Grazing Efficiency	0.7	-	0.3−0.7
m_1	Microzooplankton Mortality in the Absence of DMS	0.1	$days^{-1}$	0.015 − 0.15
m_2	Zooplankton Mortality in the Absence of DMS	0.15	$days^{-1}$	0.015 − 0.15
m_3	Chemical Evaporation or Flux to the Atmosphere	0.03	$days^{-1}$	

η	DMS Production Rate	0.1	-	
β	Mesozooplankton Linear Predation Term	1	-	
ζ	Chemical Release, Rate of Increase	C_P	-	
ω	Exotic Rate for each Phytoplankton Cell	0.01	-	

6. Mathematical analysis and results

6.1. Time Series and Phase Portraits

The main objective of this section is to support the analytical findings with the help of experimental parameter values derived from the published literature — as presented in table 2. This table is of the 14 parameters used in the model 10 across the same range as the range of the parameters shown in my previous work on two species spatial analysis. Also the values of these parameters are closely related to the value of the main control parameters, v and m_3, that helped us to set initial condition/prediction (IC) for the numerical analysis (in order to obtain consistent results). One of the main purposes of this section is to verify our analytical findings (in Table 3) using numerical methods. The numerical simulations illustrate a number of important features of the system from a practical point of view. Figure 3 exhibits the local stability of the model around a proposed initial condition; we set this condition in order to test the consistency between the two species model and the expanded model (with the parameter values given in table 2).

In figure 3, the development over time plot is of the special case model and the trajectory in *PMZC* space of the system from the proposed initial condition (P_e,M_e,Z_e,C_e) = (3.942,5.789,0.0481,20.379) and $\zeta = 0.01$ (and all other parameters fixed at their default values). In 3(b), it is shown that the trajectory is attracted onto a limit cycle with a specific period of roughly 500 days. The trajectory exhibits large-amplitude fluctuations in *P*.

The dynamics of the prey-dependent model are: stable coexistence, unstable coexistence, or extinction of the predator.

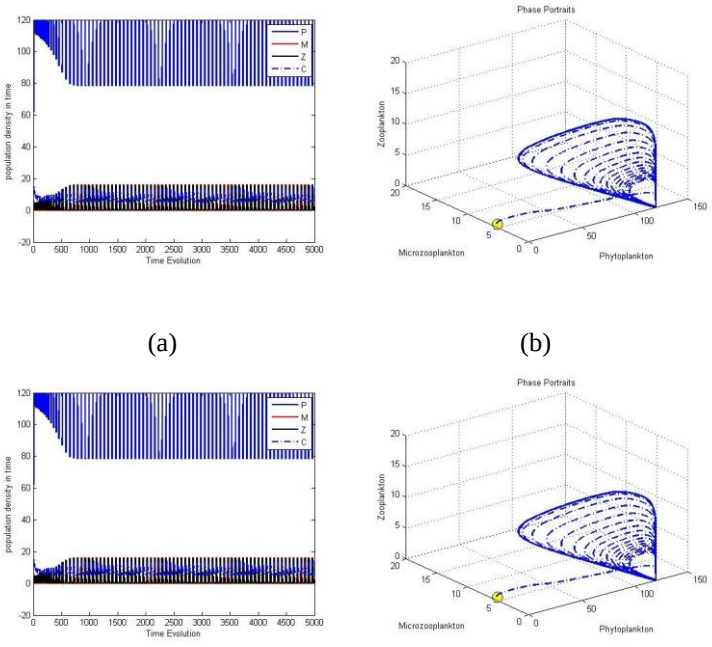

(a) (b)

(c) (d)

Figure 3: Time series and phase-space trajectories around the proposed initial condition for the two cases of *PMZC* system put forward here: all of the other parameters (not included in the set initial condition) are fixed as in table 2 — also $\zeta = 0.01$. In both cases, the trajectories are attracted to the equilibrium point, and this results in a stable limit cycle.

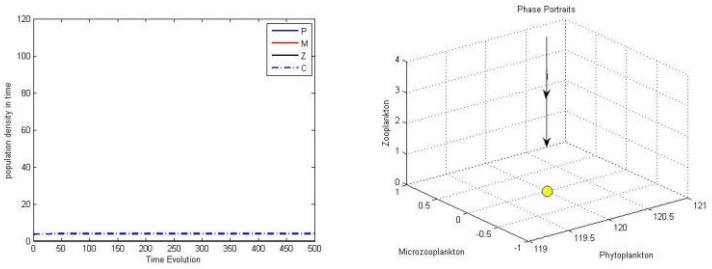

(a) (b)

Figure 4: Time series and phase portraits near the microzooplankton and copepod eradication equilibrium point, E_1 and ζ = 0.01.It is readily seen that the trajectories are attracted onto a stable limit cycle

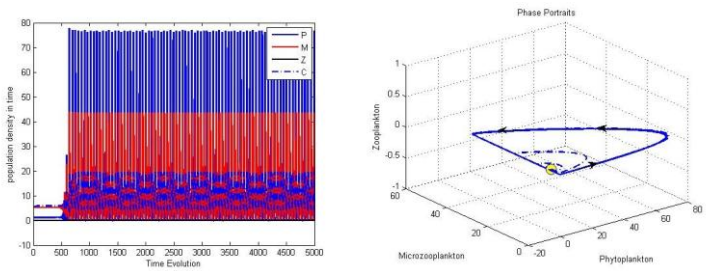

(a) (b)

Figure 5: Time series and phase portraits of (copepod free) equilibrium point E_3 withζ = 0.01 and all other parameters fixed as in 2. The trajectories are attracted onto a stable limit cycle.

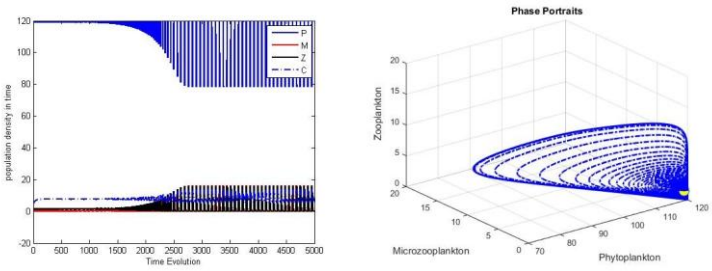

(a) (b)

Figure 6: Time Series and phase portraits around the coexistence equilibrium point E_4 with ζ = 0.01 and all the other parameters fixed at their default values and In 6(a), the limit-cycle components for the PMZC model is shown in red, blue, dashed blue

and in black. The limit-cycle represents the overall movement over the time series, ignoring seasonality and any small random fluctuations. In 6(b), It is illustrated that the trajectories are attracted onto a stable limit cycle.

6.2. One parameter bifurcation behaviour

We have used numerical simulations of the proposed model 10. Figure 7 represents the local stability diagram around E_4 with the parameter values given in table 2. It is readily seen that 7(a) indicates that if in the coexistence equilibrium $E_4 < K$ then the population of phytoplankton will bloom. Especially, if E_4 is a function of ζ; this can be seen to reflect the consistency between our previous work and this current study. However, if $E_4 > K$ then the prey population will decrease significantly. Also, if $E_4 = K$ then the population will remain constant (Freedman, 1980).

These graphs illustrate the *PMZC* biological model. When a specific choice of parameters is made, the prey population increases to extremely high numbers in each cycle and then recovers (while the predator population remains sizeable as at the highest prey density). In real-life situations, how-

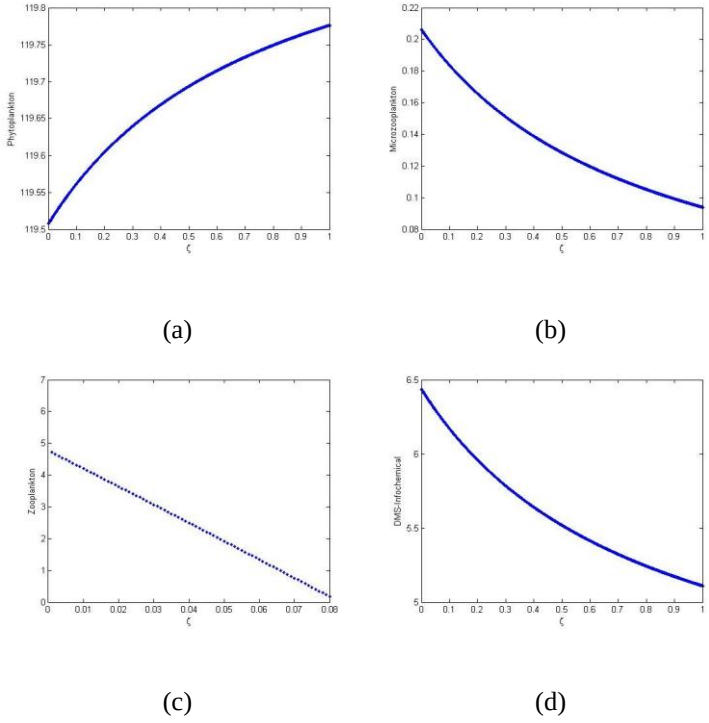

(a) (b)

(c) (d)

Figure 7: The coexistent equilibrium point w.r.t ζ as an infochemical metric, shows that the range of our control parameter should be $0 < \zeta < 0.1$ to avoid having negative real roots for Z.

ever, chance fluctuations in the discrete numbers of individual entities and in the life-cycles of prey might cause the prey to actually go extinct, and, by consequence, the predators as well (Chapman and Reiss, 1998).

7. Turing Analysis in Relation to the *PMZC* Model

Several studies have been devoted to the various modes of spatiotemporal organization generated by different models: e.g., limit cycles, Turing patterns, and traveling waves in one-dimensional systems ().The interest in this paper is to provide a fundamental understanding of how a steady state that is locally asymptotically stable in a non-spatial system can become unstable in a corresponding diffusive system. Consider the system in 1, where U_i and i = 1,2,3,4 represent a vector of the system state variables P,M,Z,C at position X and time t. It is readily seen that, in the vicinity of a spatial homogeneous steady state (P_e,M_e,Z_e,C_e), the corresponding linearized system has the following form:

$$\frac{dU_i(t)}{dt} = \sum_{j=1}^{4} a_{ij} U_j \tag{30}$$

where $U_i = P,M,Z,C$, and i = 1,..,4 this is in the case of a spatially homogeneous perturbation, and

$$\frac{d\overline{U_i}(t,k)}{dt} = \sum_{j=1}^{4} \left(a_{ij} - k^2 D_i \delta_{ij}\right) \overline{U_i}(t,k) \tag{31}$$

In the case of a spatially inhomogeneous *perturbation* with *k* as a wave number. Here $a_{ij} = \frac{\partial f_i}{\partial U_j}$ and δ_{ij} is the Kronecker symbol, and $U_i(t)$ and $U_i(t,k)$ are the amplitudes of the perturbation and its Fourier transform, respectively (Malchow, 1993). It is readily seen that when $k = 0$, the system given by 30 coincides with that in 31. The matrix of the linearised system is shown in Appendix B. We obtained the dispersion relation as a quartic polynomial and by solving this polynomial for δ we can study the Turing
instability conditions.

$$\sum_{i=0}^{4} P_i \delta^{4-i} = 0 \quad , \qquad (32)$$

Where P_i are all cascading parameters, all the related details are given in Appendix C. It is apparent that, according to the analytical break-down shown in table 3, E_1 is a steady state of the system 10, called the phytoplankton and infochemical equilibrium. This state is stable under the common two conditions *trace*(*A*) < 0 and $a_{11} + a_{22} + a_{33} + a_{44} < 0$. Spatiotemporal chaos arises from the diffusive coupling of local limit cycle oscillators (Malchow et al., 2008); the patterns so generated in two- and three-dimensional systems include patterns arising from the interference of different instability mechanisms.

8. Spatial Distribution and Limit Cycles

In this section we consider the model in Eq. (1) as it exists in continuous time and space. The model is of four interacting species and represents an example of a community population with an oscillatory solution. Here we are interested in the possible emergence of non-Turing, Turing, and limit cycle patterns. First, we assume that the diffusivity is the same for all species, and then we assume that $D_C < D_M < D_Z < D_P$. However, it appears that the choice of initial condition, as given in Eq. (33), could affect the types of pattern which is generated (Murray, 2002). Fig's 8 and 9 show the one dimensional systematic analysis of Eq. (1), starting from the types of the patterns and the behaviour of the system in time and space. The PMZC model can generate a number of quite different patterns, depending on the choice of initial condition.

$$\overline{U(x,0)} = U_e + \epsilon \cos(wx). \qquad (33)$$

The type of system dynamics exhibited depends significantly on the choice of the initial conditions (Malchow et al., 2008). The initial conditions given by Eq. (33) include U_e as the system coexistence point and $\epsilon \cos(xw)$ as the perturbation term — which depends on the value of and the value of *w*, the wave number. Fig. 8 shows how the initial condition develops to a smooth spatial distribution of prey and predator. The spatial distribution gradually varies over time; the local temporal behaviours of the dynamic variables, *PMZC*, are strictly periodic and depend on the limit cycle of the non-spatial system. Another type of initial condition, as presented in Eq. (34), gives chaotic non-Turing patterns — when the zero-flux boundary

$$\begin{aligned}
\overline{P}(x,y,0) &= P_e + \epsilon_1(x-0.2L_x)(x-0.8L_x) + \epsilon_2(y-0.3L_y)(y-0.7L_y), \\
\overline{M}(x,y,0) &= M_e + \epsilon_3(x-0.5L_x) + \epsilon_4(y-0.45L_y), \\
\overline{Z}(x,y,0) &= Z_e + \epsilon_1(x-0.2L_x)(x-0.8L_x) + \epsilon_2(y-0.3L_y)(y-0.7L_y) \\
\overline{C}(x,y,0) &= C_e + \epsilon_3(x-0.5L_x) + \epsilon_4(y-0.45L_y),
\end{aligned}$$

condition is imposed. Non-Turing patterns result when we perturb the initial distribution by adding terms like and δ into the two dimensional initial distribution below:,

$$\begin{aligned}
\overline{P}(x;y;0) &= P_e + {}_1(x\ \ 0{:}2L_x)(x\ \ 0{:}8L_x) + {}_2(y\ \ 0{:}3L_y)(y\ \ 0{:}7L_y); \\
\overline{M}(x;y;0) &= M_e + {}_3(x\ \ 0{:}5L_x) + {}_4(y\ \ 0{:}45L_y); \\
\overline{Z}(x;y;0) &= Z_e + {}_1(x\quad 0{:}2L_x)(x\ \ 0{:}8L_x) + {}_2(y\ \ 0{:}3L_y)(y\ \ 0{:}7L_y); \\
\overline{C}(x;y;0) &= C_e + {}_3(x\quad 0{:}5L_x) + {}_4(y\ \ 0{:}45L_y);
\end{aligned} \tag{34}$$

Where the values for the important terms, and δ in Eqs. (34) are given as follows:

$$\epsilon_1 = -2.10^{-7}, \epsilon_2 = -6.10^{-7}, \epsilon_3 = -3.10^{-5}, \epsilon_4 = -6.10^{-5}$$

(Malchow et al., 2008).

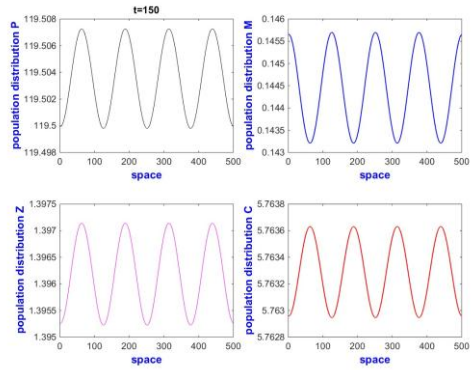
t=150
population distribution P
population distribution M
population distribution Z
population distribution C
space

(a)

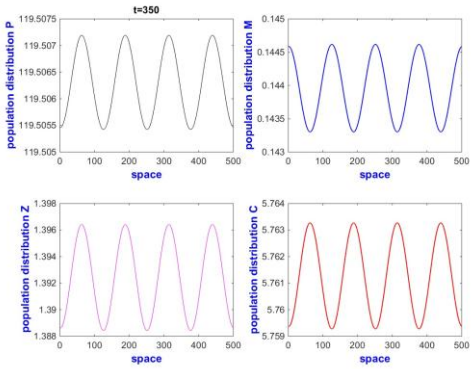
t=350
population distribution P
population distribution M
population distribution Z
population distribution C
space

(b)

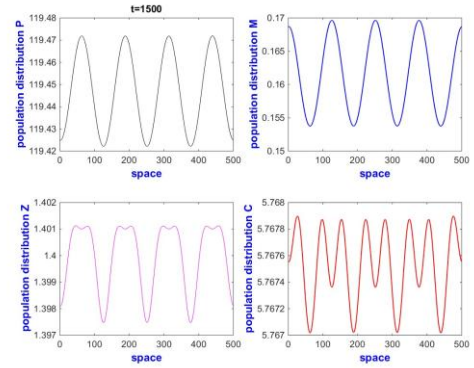
t=1500
population distribution P
population distribution M
population distribution Z
population distribution C
space

(c)

Figure 8: Population distribution over the one-dimensional space at the point's t = 150, t = 350 and t = 1500, using Eqs. (33) as the initial condition and U_e = E_4 — with parameters as shown in Table 2.

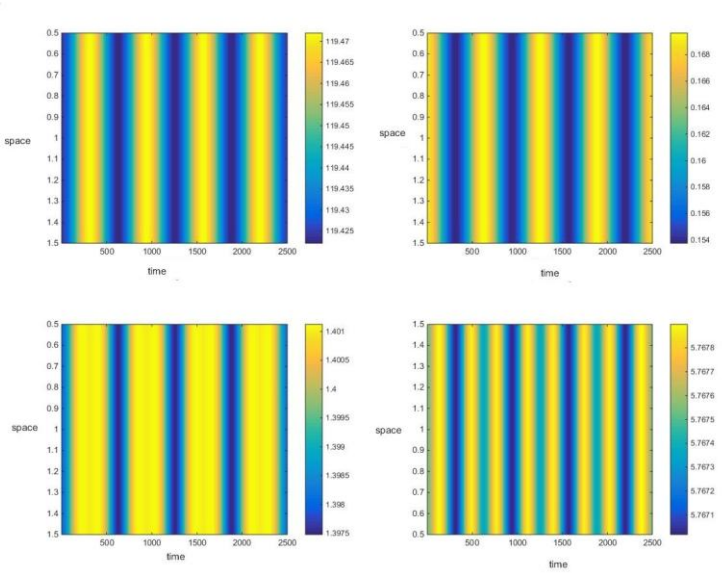

(a)

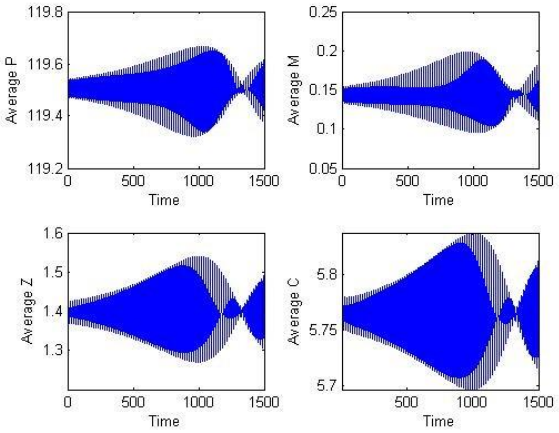

(b)

Figure 9: Schematic analysis, with respect to space and time, of Eqs. (10) and of the average density of *PMZC* in time, using Eqs. (33) as the initial condition and $U_e = E_4$.

Figures 8(a), 8(b) and 8(c) show the population densities generated by the dynamics variables at times t = 150, 350 and 1500, using $U_e = E_4$. Fig. 8(c) shows the regularity of the oscillatory solution of the population densities given by the dynamics variables in time and space. Both figures 9(a) and 9(b) in 9 illustrate regular spatiotemporal oscillations over the whole domain. Furthermore, we decided to analyse each equilibrium point of the four species model, and we present the results of these analyses in Fig. 10 and Fig. 11, for $U_e = E_3$ and $U_e = E_1$ respectively.

(a)

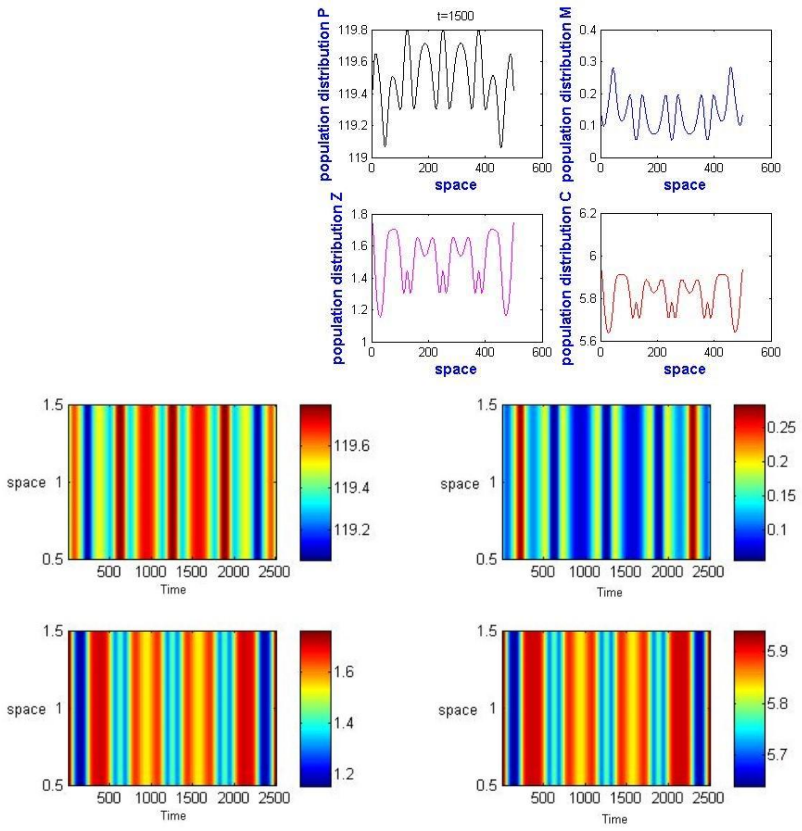

(b)

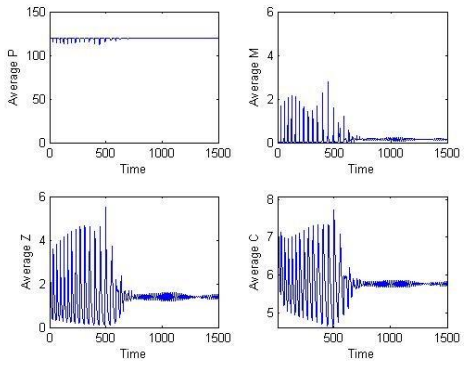

(c)

Figure 10: The population distribution over the one-dimensional space at the point33 t = 1500, plus the correspondent schematics analysis across space and time, Eqs. (10); also the average density of *PMZC* over time, using Eqs. (33) as the initial condition, E_3, for $\zeta = 0.001$ — other parameters are as shown in 2.

(a)

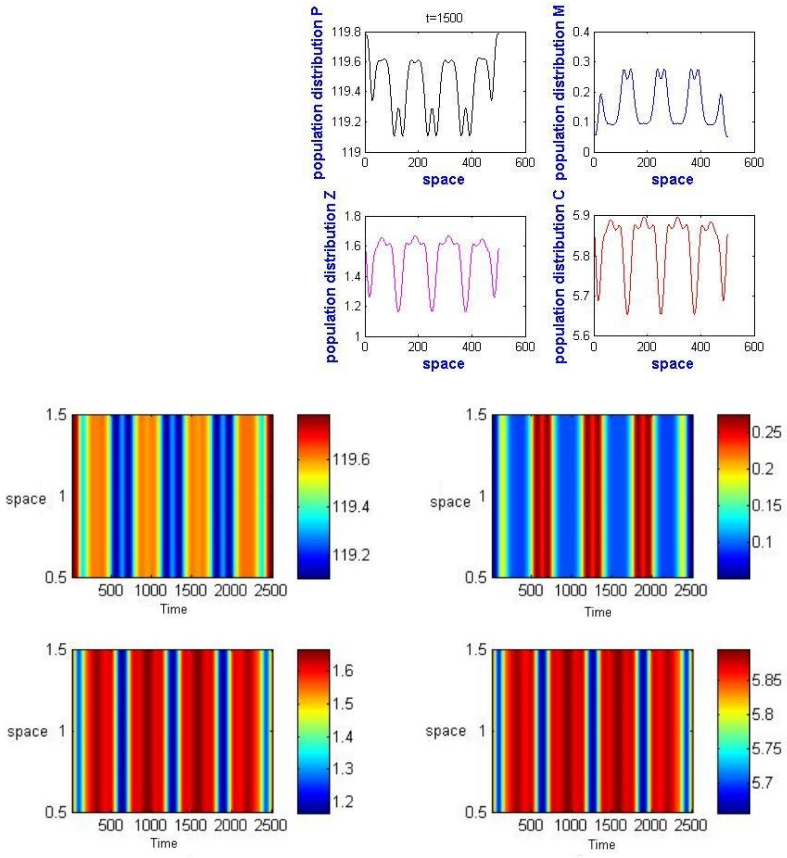
t=1500
population distribution P
population distribution M
population distribution Z
population distribution C
space
Time

(b)

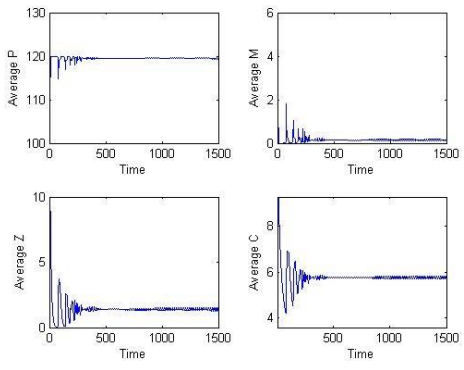
Average P
Average M
Average Z
Average C
Time

(c)

34

Figure 11: The population distribution over the one dimensional space at the point t = 1500 plus the correspondent schematics analysis across space and time, Eqs. (10); also the average density of *PMZC* over time, using Eqs. (33) as the initial condition, E_1, for $\zeta = 0.001$; other parameters are as in 2.

(a) (b)

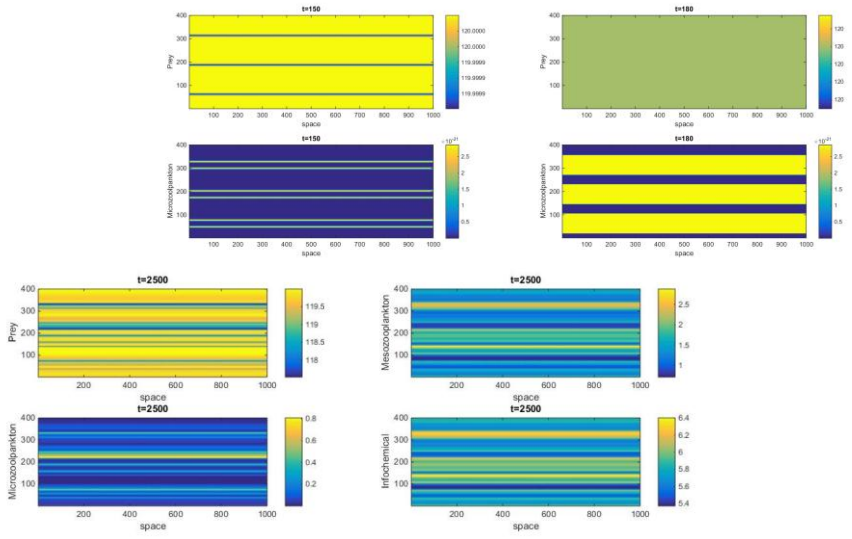

(c) (d)

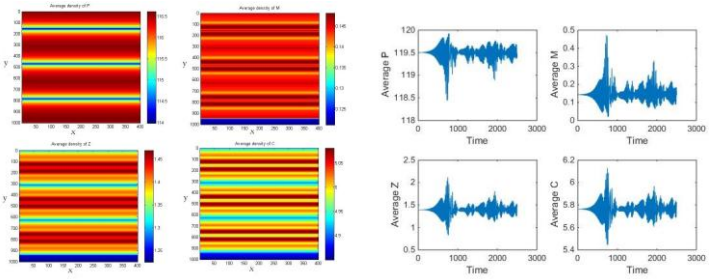

(e) (f)

Figure 12: Non-Turing patterns in a predator-prey distribution over the two dimensional space relating to the times t = 150, t = 180 and t = 1500, using Eq. (33) as the initial condition and $U_e = E_4$, with parameters as shown in Table 2. In Fig .12, the spatial distributions of a prey species at different times is presented in order to show the continuous changes in the distribution of species. Patterns are presented here which were generated within the time span t = 10 to t = 1500, but the existence of similar patterns was verified for longer duration simulations. This type of pattern is classified as a stripes patterns and is a non-Turing pattern because not all the Turing conditions hold. In Fig. 13, we find another non-Turing pattern, generated by the PMZC model when $\zeta = 0.001$ and when a suitable choice of the parameters such that $D_C < D_M < D_Z < D_P$ was made; this analysis was to include horizontal diffusion: i.e., we also consider the effects of the diffusion of *P*, *M*, *Z* and *C* in the *x*-direction. We have observed that the stationary nonTuring patterns are cold spot patterns which exhibit circular patches that have lower

concentrations of both prey and predators. The non-Turing patterns observed for the classical Holling-functional response are of two types: hot spot patterns and cold spot patterns. Hot spots consist of localized circular patches with high population densities. Our stationary cold spot pattern changed to a chaos pattern due to the coalescence of nearby circular patches with low population densities. The stationary patterns obtained for the PMZC model are completely independent of the initial condition. We have checked this independence numerically, by using E_4 as an initial guess, without perturbing it, we obtained a flat state. This unstable steady-state property of the non-stationary patterns is illustrated in Fig.12 and 13, where the spatial averages of the population densities are plotted against the space dimension, as in 12(e), and against the time dimension, as in 12(f). It is

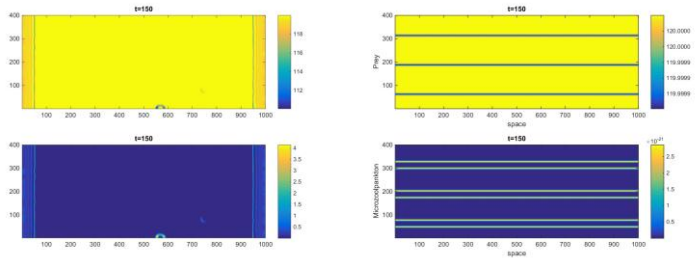

(a) (b)

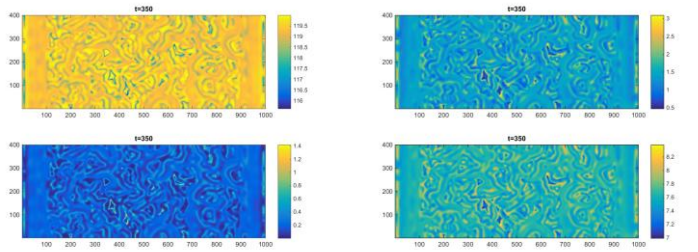

(c) (d)

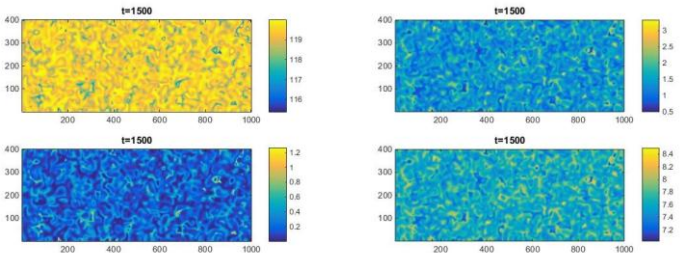

(e) (f)

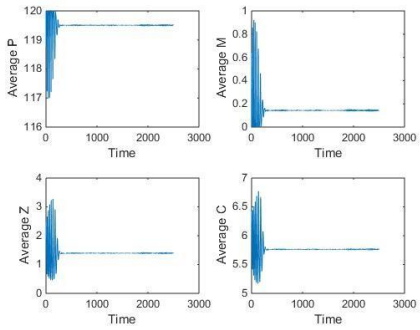

(g)

Figure 13: Non-Turing patterns for predator-prey distribution over a two dimensional space representing prey and predator for t = 150,350 and t = 1500, using Eq.34 as I.C. with $U_e = E_4$ and $\zeta = 0.001$; all other parameters are as shown in Table 2.

Important to note here that the temporal steady state is unstable and oscillates for $\zeta \geq 0.001$. Further analysis is performed in order to investigate other biologically relevant equilibria which were generated in order to obtain some specific patterns; the patterns yielded vary according to the choice of the initial condition and the type of the equilibrium. See Fig. (14).

The patterns produced by the PMZC model 1 can be in the form of a stripe-like arrangement of activated cells (in terms of phytoplankton concentrations)[3]; alternatively, active spots can lead to chaos. E_1,E_3 and E_4 are unstable equilibriums of the non-spatial model: Eqs.7–, 10, $\Rightarrow <(\lambda) > 0$. The Turing conditions are not satisfied and this gives rise to chaos patterns in the spatial system because $\Rightarrow \lambda(k^2) > 0$. Spatiotemporal chaos arises from a diffusive coupling system of equations with local limit cycle oscillators(Malchow et al., 2008); spatiotemporal patterns depend on the choice of the initial conditions. Infochemically mediated interactions can have a strong effect on the structuring, functioning and composition of marine ecosystems. For example, it has been observed that chemical gradients play a key role in generating complex patterns and in cell differentiation (Steinke et al., 2006).

[3] The concentration of the activator (P) is suggested by the dot or spot density

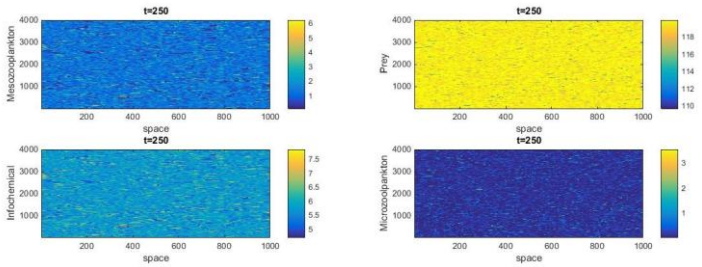

(a) (b)

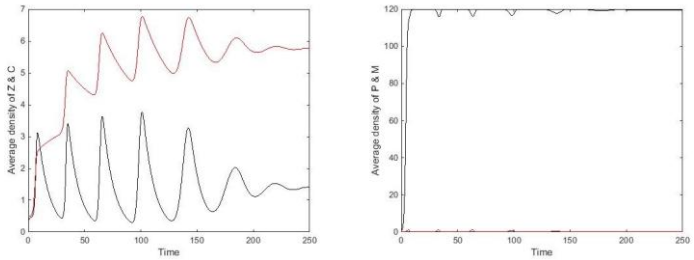

(c) (d)

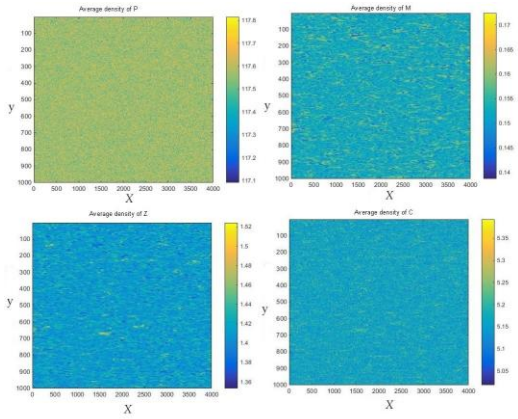

(e)

Figure 14: Non-Turing patterns generated by Eq. (1), using the initial conditions from Eq. (34) with $U_e = E_1$ and $\zeta = 0.001$; other parameters are as shown in 2.

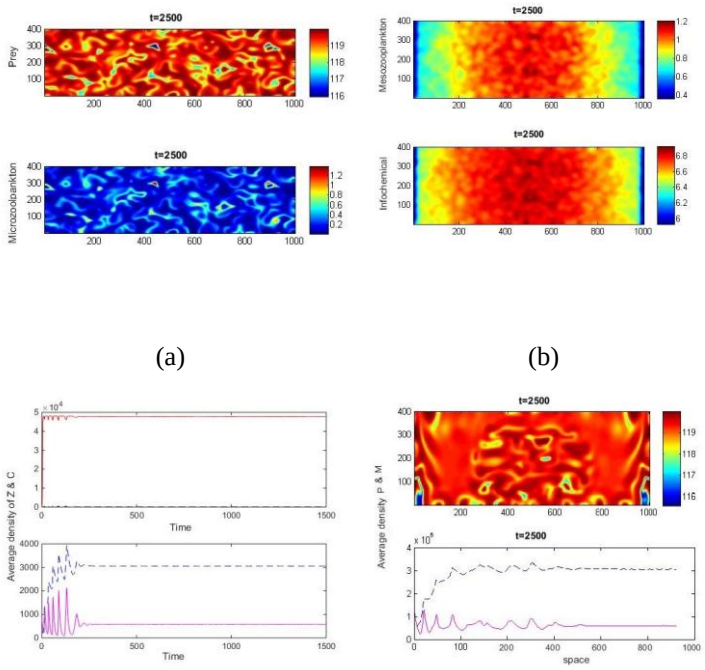

Figure 15: Non-Turing patterns generated by Eq. (1), using the initial conditions from Eq. (34) with $U_e = E_3$ and $\zeta = 0.001$; other parameters are as shown in 2.

Table 3: Spatial Analysis of the four species model presented in Eq. (1).

Equilibrium	Description	Turing Conditions	Routh–Hurwitz Criterion	Type of pat-terns
E_0	Trivial (eradication)	$\lambda(k^2) > 0$ and $H(k^2)$	$P_1 > 0$,	
E_1	Phytoplankton and infochemical equilibrium	$\lambda(k^2) > 0$ and $H(k^2) < 0$	$P_1 > 0$,	Stripes patterns using Eq.33 as I.C. and spots pattern using Eq.34 as I.C.
E_2	Biologically irrelevant equilibrium as given in Eq. (15)	$\lambda(k^2) > 0$ and $H(k^2) > 0$	$P_1 > 0$,	Stripes patterns using Eq.33 as I.C. and spots pattern using Eq.34 as I.C.
E_3	Copepod eradication equilibrium given by Eq. (16)	$\lambda(k^2) > 0$ and $H(k^2) > 0$	$P_1 > 0$,	Stripes patterns using Eq.33 as I.C. and spots pattern using Eq.34 as I.C.
E_4	Full Coexistence equilibrium given by Eq. (17)	$\lambda(k^2) > 0$ and $H(k^2) > 0$	$P_1 > 0$,	Stripes patterns using Eq.33 as I.C. and spots pattern using Eq.34 as I.C.

9. Acknowledgment

Tahani Al-Karkhi gratefully acknowledges financial support from the Ministry of Higher Education and Scientific Research in Iraq/Baghdad for the fund provided to implement this work. Also, she is grateful to her supervisors Hadi Susanto and Edward Codling for their help and support provided to improve the PMZC model and perform the results in a presentable way.

10. Conclusion

In this paper, a one prey and two predator system with Holling type II functional responses has been considered. It is shown that there exists a limit cycle with respect to the chemical release, ζ, in relation to the spatially homogeneous system as given in fig.7. In the qualitative analysis of Eq. 1, we studied the dynamical behaviour of the temporal system. It was established that when the rate of mutual interference of the predator (i.e., M and Z), crosses a threshold value (i.e., $M = M_0$ and $Z = Z_0$) then prey, first predator and second predator populations start oscillating around the interior equilibrium as shown in Fig.7. The dynamics of spatially inhomogeneous aquatic communities has been illustrated in this chapter by studying Turing instability in the *PMZC* model, using the Routh Hurwitz criteria (DeJesus and Kaufman, 1987). The Turing criteria did not hold in relation to this study because, as we have remarked earlier, the coexistence point, E_4, possesses four eigenvalues and two of these represent an unstable focus (with $Re(\lambda) > 0$) and the other two stable sinks. Furthermore, based on the numerical experiments, we obtained a spatial homogeneity in Eq. (10) which can give way to the appearance of a regular spatiotemporal pattern, depending on the parameter range given in Table 2. It is important to clarify that spatiotemporal chaos is typical for two dimensional reaction-diffusion systems with oscillatory dynamics. However, oscillatory behaviour is seen in the four species model even with small amplitudes in Eq. (1), and can be seen to be widely possible in terms of the response of the plankton model over time and space. Different patterns may be obtained by setting different initial conditions and using different numerical methods. We address the issue of the non-Turing patterns in Figs. 12 and 13 –using different initial conditions for the reaction–diffusion PMZC model (one and two dimensional). The population densities of all the species illustrated in Fig. 12 showed oscillatory behaviour; this behaviour raises an important question in relation to the phytoplankton population response to the periodic (seasonal) stimuli (Ryabchenko et al., 1997). Such large scale oscillations may push the system into and out of oscillatory phase during the course of the year (Edwards and Brindley, 1996). The models short-term oscillations are connected with feedbacks in the ecosystem initiated either by abrupt changes in the phytoplankton, by increased density in spring or by increased spatial depth in autumn (Ryabchenko et al., 1997). The systematic analyses of the nonlocal interactions in the one dimensional model of Fig. 9 and in the two dimensional model of Fig. 12 prove the persistence of the oscillation that we have already discovered in the spatially homogeneous model and show the consistency between the density and the average. In relation to this, for mathematical simplicity, the ranges of the nonlocal interactions for prey and predators are assumed to be same (this is consistent with (Banerjee and

Banerjee, 2012)). Also, we could provide a more detailed explanation of the sort of patterns that were yielded by studying further the dispersion relation of the model as it is when we obtain the striped patterns given in Fig. 12, because we used a periodic function as an initial condition for Eq. (33). As found in (Genieys et al., 2006), we can expect the existence of oscillatory travelling waves and more complex, for instance modulated, spatio–temporal dynamics. Spatiotemporal patterns exists for the parameter values given in Table 2. In Fig 13, using the parameter values shown in Table 2 but different initial conditions such as the initial conditions given in Eq. (34), we observed a pattern formation with a number of different time steps. Also, it can be observed that the stationary "mixtures $-\!\!\rightarrow$ stripe–spot mixtures $-\!\!\rightarrow$ spots" patterns are time-dependent, as was found in (Malchow et al., 2008). These observations confirm the fact that the interactions between the temporal and the spatial aspects are unable to drive the system towards spatial and temporal irregularity under any circumstances. The existence of irregular distributions of populations over space and continuous changes to these over time depends on complex interactions which take place over both the spatial and temporal scales. Finally, all these spatial patterns show that qualitative changes lead to different spatial density distributions for each species, across the spatial system. Furthermore, we analysed the stability of the linear and non-linear systems with the help of a Turing instability analysis and observed that the spatiotemporal system in Eq. (1) does not change its behaviour: as revealed by the spatial systematic analyses shown in Figs. 8 and 9 for one dimension; and Figs. 12, 12(e), 12(f), 13 and 13(g) for two dimensions. This is because the trajectories are spiralling in a limit cycle and thus they tend to converge into a stable point. Our results show that modeling by reaction –diffusion equation is an appropriate way to investigate the fundamental mechanisms of the spatio-temporal dynamics of the real world food web system (Petrovskii and Malchow, 1999) and (Baghel et al., 2014).

11. Appendix

A. The cascading parameters of the coexistence point

$$A_0 = \gamma_2 b_1 \beta \eta r^2 + \zeta b_1 \beta \eta r^2 - b_1 b_2 \eta m_2 r^2,$$

$$A_1 = -2\gamma_2 b_1 \beta \eta k r^2 - 2\zeta b_1 \beta \eta k r^2 + 2 b_1 b_2 \eta k m_2 r^2 - \gamma_2 b_1 \beta k \omega r - \zeta b_1 \beta k \omega r$$

$$+ b_1 b_2 k m_2 \omega r + \gamma_2 \beta \eta r^2 + \zeta \beta \eta r^2 - b_2 \eta m_2 r^2,$$

$$A2 = -\gamma 2 b1 \beta \eta k2 r2 + \zeta b1 \beta \eta k2 r2 - b1 b2 \eta k2 m2 r2 + \gamma 2 b1 \beta k2 \omega r$$

$$+ \zeta b_1 \beta k^2 \omega r - b_1 b_2 k^2 m_2 \omega r - \gamma_2 b_1 \beta k m_3 r - 2\gamma_2 \beta \eta k r^2 - 2\zeta \beta \eta k r^2$$

$$+ b_1b_2km_2m_3r + 2b_2\eta km_2r^2 - \gamma_2\beta k\omega r - \zeta\beta k\omega r + a\eta km_2r + b_2km_2\omega r,$$

$$A3 = \gamma 2b1\beta k2rm3 + \gamma 2\beta\eta k2r2 + \zeta\beta\eta k2r2 - b1b2k2rm2m3$$

$$- b_2\eta k^2r^2m_2 + \gamma_2\beta k^2\omega r + \zeta\beta k^2\omega r - a\eta k^2rm_2 - b_2k^2\omega rm_2$$

$$- \gamma_2\beta krm_3 - ak^2\omega m_2 + b_2krm_2m_3,$$

$$A4 = \gamma 2\beta k2m3r - b2k2m2m3r - ak2m2m3,$$

B. The details of the fourth eigenvalue correspond to E_2

$$A_0 = \gamma_1ak(\gamma_1a - b_1m_1) \quad \text{(B.1)}$$

$$\alpha = -m_1(\gamma_1ab_1kr + b_1^2km_1r + r\gamma_1a + b_1m_1r)$$

$$\beta = -4\gamma_1^4a^4k^2m_1r + 12\gamma_1^3a^3b_1k^2m_1^2r - 12\gamma_1^2a^2b_1^2k^2m_1^3r$$

$$+ \gamma 12a2b21k2m21r2 + 4\gamma 1ab13k2m14r - 2\gamma 1ab31k2m31r2$$

$$+ b41k2m41r2 + 4\gamma 13a3km21r - 8\gamma 12a2b1km31r$$

$$- 2\gamma 12a2b1km21r2 + 4\gamma 1ab21km14r + 2b31km41r2$$

$$+ \gamma 12a2m21r2 + 2\gamma 1ab1m31r2$$

$$+ b21m41r2$$

C. The cascading value of A and B of the eigenvalue -correspond to the equilibria E_3.

$$A = -\gamma 14\gamma 2a3\beta k2m3r + \gamma 14a3b2k2m2m3r + 3\gamma 13\gamma 2a2b1\beta k2m1m3r$$

$$- \gamma 13\gamma 2a2\beta\eta k2m1r2 - \gamma 13\zeta a2\beta\eta k2m1r2$$

$$- 3\gamma 13a2b1b2k2m1m2m3r + \gamma 13a2b2\eta k2m1m2r2 - 3\gamma 12\gamma 2ab12\beta k2m21m3r$$

$$+ 2\gamma 12\gamma 2ab1\beta\eta k2m21r2 + 2\gamma 12\zeta ab1\beta\eta k2m21r2$$

$$+ 3\gamma 12ab21b2k2m21m2m3r - 2\gamma 12ab1b2\eta k2m21m2r2 + \gamma 1\gamma 2b31\beta k2m31m3r$$

$$+ \gamma 1\gamma 2b21\beta\eta k2m31r2 - \gamma 1\zeta b21\beta\eta k2m13r2 + \gamma 1b31b2k2m31m2m3r$$

$$+ \gamma 1b21b2\eta k2m31m2r2 + \gamma 14a4k2m2m3 - \gamma 13\gamma 2a2\beta k2m1\omega r$$

$$- \gamma 13\zeta a2\beta k2m1\omega r + 4\gamma 13a3b1k2m1m2m3 - \gamma 13a3\eta k2m1m2r + \gamma 13a2b2k2m1m2\omega r -$$
$$2\gamma 12\gamma 2ab1\beta k2m12\omega r - 2\gamma 12\zeta ab1\beta k2m21\omega r$$
$$+ 6\gamma 12a2b21k2m21m2m3 + 3\gamma 12a2b1\eta k2m21m2r + 2\gamma 12ab1b2k2m12m2\omega r$$

$$- \gamma 1\gamma 2b21\beta k2m31\omega r + \gamma 1\zeta b21\beta k2m31\omega r + 4\gamma 1ab31k2m31m2m3$$

$$+ 3\gamma 1ab21\eta k2m31m2r - \gamma 1b21b2k2m13m2\omega r - b41k2m41m2m3$$

$$- b31\eta k2m41m2r - \gamma 13\gamma 2a2\beta km1m3r - \gamma 13a3k2m1m2\omega$$

$$- \gamma 13a2b2km1m2m3r + 2\gamma 12\gamma 2ab1\beta km12m3r - 2\gamma 12\gamma 2a\beta\eta km21r2$$

$$+ 2\gamma 12\zeta a\beta\eta km21r2 - 3\gamma 12a2b1k2m21m2\omega - 2\gamma 12ab1b2km12m2m3r$$

$$- 2\gamma 12ab2\eta km21m2r2 + \gamma 1\gamma 2b21\beta km31m3r - 2\gamma 1\gamma 2b1\beta\eta km31r2$$

$$- 2\gamma 1\zeta b1\beta\eta km31r2 + 3\gamma 1ab21k2m31m2\omega - \gamma 1b21b2km13m2m3r$$

$$+ 2\gamma 1b1b2\eta km31m2r2 - b31k2m41m2\omega - \gamma 12\gamma 2a\beta km21\omega r$$

$$+ \gamma 12\zeta a\beta km21\omega r - \gamma 12a2\eta km21m2r - \gamma 12ab2km21m2\omega r$$

$$- \gamma_1\gamma_2 b_1\beta km^3{}_1\omega r - \gamma_1\zeta b_1\beta km_1{}^3\omega r + 2\gamma_1 ab_1\eta km^3{}_1m_2r + \gamma 1b1b2km31m2\omega r - b21\eta km41m248r -$$
$$\gamma 1\gamma 2\beta\eta m13r2 - \gamma 1\zeta\beta\eta m13r2$$
$$- \gamma 1b2\eta m31m2r2.$$

$$B = \gamma 14a3b2k2m3r - 3\gamma 13a2b1b2k2m1m3r + \gamma 13a2b2\eta k2m1r2 + 3\gamma 12ab21b2k2m21m3r -$$
$$2\gamma 12ab1b2\eta k2m21r2 - \gamma 1b31b2k2m31m3r$$
$$+ \gamma 1b21b2\eta k2m31r2 + \gamma 14a4k2m3 - 4\gamma 13a3b1k2m1m3 + \gamma 13a3\eta k2m1r$$

$$+ \gamma 13a2b2k2m1\omega r + 6\gamma 12a2b21k2m21m3 - 3\gamma 12a2b1\eta k2m12r$$

$$- 2\gamma 12ab1b2k2m21\omega r - 4\gamma 1ab31k2m13m3 + 3\gamma 1ab21\eta k2m31r$$

$$+ \gamma 1b21b2k2m31\omega r + b41k2m41m3 - b31\eta k2m41r + \gamma 13a3k2m1\omega$$

$$- \gamma 13a2b2km1m3r - 3\gamma 12a2b1k2m12\omega + 2\gamma 12ab1b2km21m3r$$

$$- 2\gamma 12ab2\eta km21r2 + 3\gamma 1ab21k2m31\omega - \gamma 1b21b2km31m3r$$

$$+ 2\gamma 1b1b2\eta km31r2 - b31k2m41\omega - \gamma 12a2\eta km21r - \gamma 12ab2km21\omega r$$

$$+ 2\gamma 1ab1\eta km31r + \gamma 1b1b2km31\omega r - b21\eta km41r + \gamma 1b2\eta m31r2$$

D. The cascading parameter of the coexistence eigenvalue E_4

$$A1 = -a11 - a22 - a33 - a44. \qquad \text{(D.1)}$$

$$A2 = a11a22+a11a33+a11a44-a12a21+a22a33+a22a44-a23a32-a24a42+33a44.$$

(D.2)

$A3 = -a11a22a33 - a11a22a44 + a11a23a32 + a11a24a42 - a11a33a44 + a12a21a33 + a12a21a44 - a12a24a41 - a22a33a44 + a23a32a44 - a23a34a42 + 24\ a33a42.$

(D.3)$A4 = a11a22a33a44 - a11a23a32a44 + 11\ a23a34a42 - a11a24a33a42 - a12a21a33a44$

$- a12a23a34a41 + a12a24a33a41.$ (D.4)

E. References

Baghel, R. S., Dhar, J., Berezowski, M., Lawnik, M., Berzig, M., Rus, M.-D.,

Huseyin, A., Jachimavi˘ciene˙, J., Sapagovas, M., Stikonas, A., et al., 2014.˘ Pattern formation in three species food web model in spatiotemporal domain with beddingtondeangelis functional response. Nonlinear Anal Model Control 19, 155–171.

Bandyopadhyay, M., Chattopadhyay, J., 2005. Ratio-dependent predator– prey model: effect of environmental fluctuation and stability. Nonlinearity 18 (2), 913.

Banerjee, M., 2010. Self-replication of spatial patterns in a ratio-dependent predator–prey model. Mathematical and Computer Modelling 51 (1-2), 44–52.

Banerjee, M., 2015. Turing and non-turing patterns in two-dimensional preypredator models. In: Applications of Chaos and Nonlinear Dynamics in Science and Engineering-Vol. 4. Springer, pp. 257–280.

Banerjee, M., Banerjee, S., 2012. Turing instabilities and spatio-temporal chaos in ratio-dependent holling–tanner model. Mathematical biosciences 236 (1), 64–76.

Banerjee, M., Venturino, E., 2011. A phytoplankton–toxic phytoplankton– zooplankton model. Ecological Complexity 8 (3), 239–248.

Baurmann, M., Ebenhoh, W., Feudel, U., 2004. Turing instabilities and pattern formation in a benthic nutrient-microoganism system. Mathematical biosciences and engineering: MBE 1 (1), 111–130.

Cantrell, R. S., Cosner, C., 2004. Spatial ecology via reaction-diffusion equations. John Wiley & Sons.

Chapman, J. L., Reiss, M. J., 1998. Ecology: principles and applications. Cambridge University Press.

DeJesus, E. X., Kaufman, C., 1987. Routh-hurwitz criterion in the examination of eigenvalues of a system of nonlinear ordinary differential equations. Physical Review A 35 (12), 5288.

E, M., Pompei, Charlson, P., Ales, K. L., MacKenzie, C. R., 1987. A new method of classifying prognostic comorbidity in longitudinal studies: development and validation. Journal of chronic diseases 40 (5), 373–383.

Edwards, A. M., Brindley, J., 1996. Oscillatory behaviour in a threecomponent plankton population model. Dynamics and stability of Systems 11 (4), 347–370.

Edwards, A. M., Brindley, J., 1999. Zooplankton mortality and the dynamical behaviour of plankton population models. Bulletin of mathematical biology 61 (2), 303–339.

Edwards, A. M., Yool, A., 2000. The role of higher predation in plankton population models. Journal of Plankton Research 22 (6), 1085–1112.

Franks, P. J., 2001. Phytoplankton blooms in a fluctuating environment: the roles of plankton response time scales and grazing. Journal of Plankton
Research 23 (12), 1433–1441.

Freedman, H. I., 1980. Deterministic mathematical models in population ecology. Vol. 57. Marcel Dekker Inc.

Genieys, S., Volpert, V., Auger, P., 2006. Pattern and waves for a model in population dynamics with nonlocal consumption of resources. Mathematical Modelling of Natural Phenomena 1 (1), 63–80.

Holling, C. S., 1965. The functional response of predators to prey density and its role in mimicry and population regulation. Memoirs of the Entomological Society of Canada 97 (S45), 5–60.

K, P., Benson, Maini, D. L., Sherratt, J. A., 1992. Pattern formation in reaction-diffusion models with spatially inhomogeneous diffusion coefficients. Mathematical Medicine and Biology: A Journal of the IMA 9 (3), 197–213.

Kiørboe, T., 2008. A mechanistic approach to plankton ecology. Princeton University Press.

Lewis, N. D., Breckels, M. N., Archer, S. D., Morozov, A., Pitchford, J. W., Steinke, M., Codling, E. A., 2012. Grazing-induced production of dms can stabilize food-web dynamics and promote the formation of phytoplankton blooms in a multitrophic plankton model. Biogeochemistry 110 (1-3), 303– 313.

Maini, P. K., Woolley, T. E., Baker, R. E., Gaffney, E. A., Lee, S. S., 2012. Turing's model for biological pattern formation and the robustness problem. Interface focus 2 (4), 487–496.

Malchow, H., 1993. Spatio-temporal pattern formation in nonlinear nonequilibrium plankton dynamics. Proceedings of the Royal Society of London. Series B: Biological Sciences 251 (1331), 103–109.

Malchow, H., Petrovskii, S. V., Venturino, E., 2008. Spatiotemporal patterns in ecology and epidemiology: theory, models, and simulation. Chapman & Hall/CRC Press London.

Morozov, A., Arashkevich, E., Nikishina, A., Solovyev, K., 2010. Nutrientrich plankton communities stabilized via predator–prey interactions: revisiting the role of vertical heterogeneity. Mathematical Medicine and Biology, dqq010.

Murray, J. D., 2002. Mathematical Biology I: An Introduction, vol. 17 of Interdisciplinary Applied Mathematics. Springer, New York, NY, USA,.

Petrovskii, S. V., Malchow, H., 1999. A minimal model of pattern formation in a prey-predator system. Mathematical and Computer Modelling 29 (8), 49–63.

Porter, B., 1968. Stability criteria for linear dynamical systems. Academic Press.

Rosenzweig, M. L., MacArthur, R. H., 1963. Graphical representation and stability conditions of predator-prey interactions. American Naturalist, 209–223.

Ryabchenko, V., Fasham, M., Kagan, B., Popova, E., 1997. What causes short-term oscillations in ecosystem models of the ocean mixed layer?
Journal of Marine Systems 13 (1-4), 33–50.

S, C., Putman, Endres, N. F., Ernst, D. A., Kurth, J. A., Lohmann, C. M., Lohmann, K. J., 2016. Multi-modal homing in sea turtles: modeling dual use of geomagnetic and chemical cues in island-finding. Frontiers in behavioral neuroscience 10, 19.

Saiz, E., Calbet, A., 2007. Scaling of feeding in marine calanoid copepods. Limnology and Oceanography 52 (2), 668–675.

Steinke, M., Stefels, J., Stamhuis, E., 2006. Dimethyl sulfide triggers search behavior in copepods. Limnology and oceanography 51 (4), 1925–1930.

Strom, S. L., Morello, T. A., 1998. Comparative growth rates and yields of ciliates and heterotrophic dinoflagellates. Journal of Plankton Research 20 (3), 571–584.

Wolfe, G. V., Steinke, M., 1996. Grazing-activated production of dimethyl sulfide (dms) by two clones of emiliania huxleyi. Limnology and Oceanography 41 (6), 1151–1160.